Determination of Interaction Kinetics between the T Cell Receptor and Peptide-Loaded MHC Class II via Single-Molecule Diffusion Measurements

Markus Axmann,[†] Johannes B. Huppa,[‡] Mark M. Davis,[§] and Gerhard J. Schütz[†¶]

[†]Biophysics Institute, Johannes-Kepler-University Linz, Linz, Austria; [‡]Department of Microbiology and Immunology, Stanford School of Medicine, Stanford, California; [§]Howard Hughes Medical Institute, Stanford, California; and [¶]Vienna University of Technology, Institute of Applied Physics, Vienna, Austria

Supplementary Materials

1. Methods

Proteins / Antibodies

Peptides were synthesized by the Beckman Center Protein and Nucleic Acid Facility at Stanford Medical School, analyzed using reverse phase HPLC and mass spectroscopy and derivatized as published (1). In brief, peptide labeling was performed C-terminally with Cy5-maleimide (Q15108, GE Healthcare, USA). The labeling degree of the used peptides was determined using HPLC and LC-electrospray ionization mass spectroscopy and found to be nearly one dye per peptide. I-E^k was expressed, purified and loaded with fluorescent peptide as published (1).The loading grade with labeled peptide was determined photometrically and ranged between 45% and 65%. ICAM-1-$(His)_{12}$ and B7-1-$(His)_{12}$ were expressed as previously described (1). Their surface density was determined with the use of fluorescent derivatives of known protein:dye ratios, which had been incubated with the bilayer at the same concentration as the unlabeled molecules used for experimentation. Densities were 20 molecules/µm² for B7-1 and 15 molecules/µm² for ICAM-1. All proteins were dialyzed against PBS, 50% glycerol and stored at -20°C .

Cells

The 5c.c7 TCR αβ transgenic mice (on a B10A background) were purchased from Taconic. Lymphocytes were isolated from superficial cervical, axillary, mesenteric and inguinal lymph nodes and spleen of 6-16 weeks old 5c.c7 TCR transgenic mice and stimulated in 24-well plates in the presence of 1 µM HPLC-purified MCC peptide (ANERADLIAYLKQADK) at a density of 7.5×10^6 cells per well and 1 ml of complete medium (RPMI containing 10% FCS (Gemini, USA), 2mM L-glutamine (PAA, Austria), 100 U/ml penicillin/streptomycin (PAA, Austria), 50µM β-mercaptoethanol (Sigma-Aldrich, Germany) and 1 mM sodium pyruvate (Sigma-Aldrich, Germany)); this was considered day 1. Cells were split every 2 days 1:1 with complete medium. Additionally on day 3, 100 U/ml IL-2 (Sigma-Aldrich, Germany) was added to boost proliferation. On day 5, dead cells were removed by centrifugation through a Histopaque-1119 (Sigma-Aldrich) cushion (7 min at 2000 rpm in a Multifuge 1 S-R table top centrifuge), and resuspended in conditioned media supplemented with murine IL-2 (100 U/ml). Cells were used for experiments on day 6 and 7.

Determination of the TCR surface density

In order to determine the surface density of the 5c.c7 TCRs T cells were incubated on ice with FITC conjugated H57-Fab for 30 min on ice, washed once with cold Hanks Buffered Saline Solution (HBSS) (PAA, Austria) containing 1mM Ca^{2+} and Mg^{2+} and 2 % FCS (Gemini, USA) and measured by flow cytometry (FACS Aria, Becton Dickinson, USA). By comparison with Spherotech beads (RCP-30-5A, USA) we calculated a TCR surface density of about 40 molecules/μm^2.

In an equilibrated system, the pMHC binding of TCR molecules in the contact area would lead to TCR enrichment, which would have to be taken into account for the determination of the dissociation constant. We therefore measured TCR surface density also directly in the contact area between the T cell and the bilayer under activating conditions. For this, the TCR was labeled with a Cy3-conjugated single chain fragment (J1-Cy3 in Ref. (1)), and the average fluorescence intensity was compared with the single molecule brightness of J1-Cy3. Also in this case, we determined an average of

40 TCR molecules/μm^2 over the whole contact area. The accordance of the results indicates that the TCR surface density is regulated by the T cell, most likely by internalization of TCR in the synapse.

Supported Lipid Bilayers

Planar glass-supported lipid bilayers were prepared as published (1). In brief, vesicles containing 10% (1,2-dioleoyl-SN-Glycero-3-(N(5-amino-1-carboxypentyl) iminodiacetic acid)succinyl (DGS-NTA) in 1,2-di-oleyl-SN-glycero-3-ethylphosphocholine (POPC) (both from Avanti polar lipids, USA) were added to a clean cover glass at 25°C and incubated for 20 min; excess vesicles were washed away with PBS without exposing the surface to air. Protein master mix solutions were incubated for 1 hour in the dark to allow the different histidine-tagged proteins to attach to the Ni-NTA-head group of the DGS lipids. Unbound proteins were washed away with PBS. The surface density of proteins was determined by comparison of the single molecule signal intensity and the mean bulk fluorescence of the bilayer. Measurements were performed in HBSS containing 1mM Ca^{2+} and Mg^{2+} and 1% ovalbumin (A-5503, Sigma-Aldrich, Germany).

Microscopy

All experiments were performed on a modified Axiovert 200 epifluorescence microscope (Zeiss, Germany). Samples were illuminated in Total Internal Reflection (TIR) configuration via a 100x, NA=1.46 Apochromat objective (Zeiss) for illumination times t_{ill}=1 ms using an acousto-optic modulator (AOM 1205C-2, Isomet, USA). For selective fluorescence excitation of Cy3 at 514nm and Cy5 at 647nm an Ar^+- (Stabilite 2017-AR, Spectra Physics, USA) and Kr^+-ion laser (Stabilite 2017-KR, Spectra Physics, USA) had been used, respectively. Laser excitation was limited to the field of view using an aperture in the optical pathway. Simultaneous bright field illumination was achieved using an excitation filter (D577/10X, Chroma) in the illumination path of the HAL 100 lamp of the microscope.

Using custom filter combinations (Z520/647 RPC and Z528/647M, Chroma; 700 nm short pass, Newport, USA) the fluorescence emission was separated from the excitation light and split into two spectral channels using a dichroic wedge (1° separation, Chroma, USA) in the parallel beam path; one channel was for the (Cy5-p)MHC signal, the second for the transmission light image of the T cells. The two images were recorded on a back-illuminated, liquid-nitrogen cooled CCD camera (Micro Max 1300-PB, Roper Scientific, USA). The camera was operated in kinetics mode, which allowed short delay times t_{del} = 49 ms between consecutive images by shifting individual subimages into a masked region of the chip before reading out the whole CCD chip; the according time-lag between n images is given by $t_{lag} = n(t_{ill} + t_{del})$. In kinetics mode, the total number of images within a sequence is thus restricted by the total number of pixel-rows on the chip (i.e. 12 images with a height of 108 pixels on a chip with 1300 rows). Since a single sequence of 12 images photobleached the majority of probes in the observation area, we set a delay time of 20 s between the recording of subsequent sequences to ensure re-equilibration of the pMHC (both free and TCR-bound) in the contact area.

Experiments were performed using a custom-made heating box equipped with a control and heating unit (Temp-control 37-2 digital + heating unit, Pecon) and an objective-heater (Temp-control mini + objective heater, Pecon). Local temperature was determined precisely using a temperature probe (1521 Thermometer Readout, Fluke Hart scientific) inside the measurement chamber. Experiments were performed at 37°C, 28°C, and at 33°C (**Supplementary Data**).

Data analysis

Image analysis was performed using self-made algorithms implemented in MATLAB (MathWorks). The position of individual fluorophores imaged as diffraction limited fluorescence signals was

determined as previously described (2). Single molecule trajectories were reconstructed by a semi-automatic MATLAB routine. For the data shown in **Fig. 1** and **2**, mean square displacements (*msd*) were calculated for the whole data set, plotted against t_{lag}, and fitted with $msd = msd(0) + 4Dt_{lag}$, where $msd(0)$ gives a measure for the localization errors $\delta = \sqrt{msd(0)/4}$) and *D* is the overall diffusion constant. At least 1200 trajectories were included for determination of the individual diffusion constants.

For the testing approach shown in **Fig. 3**, all square displacements *sd* within single trajectories were determined and used to calculate the diffusion constant estimator for each single molecule $\overline{D} = \langle sd/4t_{lag} \rangle$.

Analysis of 2-dimensional binding equilibria

In our experiments we observed a constant surface density of the TCR, $\sigma_{TCR-total}$, independent of the nature of the presented peptide, and regardless of whether TCR densities were measured by flow cytometry in suspension or through TIR-illuminated fluorescence microscopy within the immune synapse. Therefore, in order to calculate the dissociation constant K_D for the pMHC-TCR-complex the following model was used:

$$TCR + pMHC \leftrightarrow TCR\text{–}pMHC$$

Assuming a two-dimensional binding equilibrium the concentration of bound complexes, $\sigma_{pMHC-bound}$, is given by

$$\sigma_{pMHC-bound} = \frac{\sigma_{TCR-total}}{1 + \frac{K_D}{\sigma_{pMHC-free}}}$$

where K_D denotes the dissociation constant, $\sigma_{TCR-total}$ and $\sigma_{pMHC-free}$ the surface density of total TCR and free pMHC, respectively. The observed diffusion constant *D* is described by a linear combination of the diffusion constants of free and bound pMHCs:

$$D = D_{free}\frac{\sigma_{pMHC-free}}{\sigma_{pMHC-total}} + D_{bound}\frac{\sigma_{pMHC-bound}}{\sigma_{pMHC-total}}$$

$\sigma_{pMHC-total}$ denotes the surface density of total *pMHC*, D_{free} and D_{bound} the diffusion constant of the free and bound pMHC. Finally, the two equations can be combined, yielding

$$D = D_{free} - \frac{D_{free} - D_{bound}}{\sigma_{pMHC-total}}\left\{\frac{K_D + \sigma_{TCR-total} + \sigma_{pMHC-total}}{2} - \sqrt{\left(\frac{K_D + \sigma_{TCR-total} + \sigma_{pMHC-total}}{2}\right)^2 - \sigma_{TCR-total}\sigma_{pMHC-total}}\right\} \qquad \text{Eq.(1)}$$

Monte Carlo Simulations & Kolmogorov-Smirnov Test

We have recently introduced a new method to extract information on a statistical pool of data, based on comprehensive testing against hypotheses covering all reasonable parameter settings (3). In the following we briefly sketch the essentials of this approach for this particular application.

The analysis is based on the statistical distribution of recorded diffusion constants, which – for visualization – can be plotted as probability density function or as histogram. The underlying idea is to compare the measured sample distribution X with a manifold of distributions Y, which are simulated on the computer for various parameter settings. The actual comparison is done with a two-sample Kolmogorov-Smirnov hypothesis test. In general, such two-sample tests are designed to assess whether two samples X and Y are drawn from the same underlying distribution (H_0 hypothesis). As an output the test yields the p-value, which is a measure of the statistical difference of the two distributions X and Y. The p-value quantifies the extremeness of a randomly drawn sample by specifying the probability of obtaining a sample at least as extreme as the one which was actually observed, assuming that H_0 is true. If we specify a significance level α such that H_0 will be accepted for α<p-value and rejected for α>p-value, then α defines the probability of falsely rejecting H_0. By calculating the p-value between X and every simulated test sample Y we get an estimate of the parameter settings which likely lead to the observed data, and of those parameters which would rarely lead to data as extreme as observed. Note that the Kolmogorov-Smirnov-test does not depend on the data representation (e.g. differently binned histograms, or probability density functions), since it is performed on the originally recorded distributions.

Here we used the testing approach to compare the statistical distribution of the measured diffusion constant estimators $\overline{D}$ with simulated data. Data set X thus contains around 1500 estimated diffusion constants; the data sets Y come from the simulations at various parameter settings. We modeled the sequence of binding and unbinding events of single pMHC molecules as a sequence of transitions between free and bound states, where the according transition lifetimes were distributed exponentially. It should be pointed out that the transitions were only modeled in time, and we disregarded any spatial information about the location of the trajectories within the IS.

As examples, we plotted histograms of $\overline{D}$ from computer-simulated data sets in **Supporting Fig. 6**. The bound fraction was set to 50%, mobilities for free and bound state, localization errors, lengths of the trajectories, and the time delay between consecutive images were chosen identical to the measured data. Panel A, B, and C show different transition times. In (**A**) we simulated a situation where transitions are much slower than the time resolution of the method ($\tau_{on} = \tau_{off} = 1s$). In this case, trajectories are essentially observed either in the bound state or in the unbound state, but transitions are hardly present. In consequence, the histogram shows well separated peaks: the right peak corresponds to the freely mobile fraction, the left peak to the bound fraction. In both cases the mobility estimator peaks at slightly right-shifted values compared to the adjusted diffusion constants due to localization errors. In (**B**) and (**C**) the time resolution of the transitions were chosen such that they matched the resolution of the recording sequence, so that transition will be present in the trajectories. Now the peaks begin to move towards each other and finally merge.

We further show simulations for a bound fraction of only 7% (similar to the results of the peptides T102S and β2m; **Supporting Fig. 7**). In this case, the bound fraction has a much lower statistical weight, yielding a rather small peak at low mobility. When times are decreased, the two peaks begin to merge again, however, there is hardly any shift in the main peak observable. Moreover, the differences between the distributions are less pronounced than in the case of 50% bound fraction, so that the discrimination of the different transition rates is difficult.

We would like to particularly point out some characteristics of the plots: i) The peak positions do not necessarily reflect the mobility of the species (for example the right peak corresponding to the free state mobility gets clearly shifted towards lower values). ii) The areas in the peaks do not necessarily reflect the weights of the fractions (see e.g. panel (**C**), where the 50% bound fraction may be underestimated at a quick look onto the plot). iii) The discriminative strength of the testing approach

is highest, when the shapes of the probability distributions are clearly discernible. For example, panels (**A**), (**B**) and (**C**) can be unambiguously discriminated ($p\text{-}values \ll 0.01$). If bound fractions become very small (e.g. 7%), however, no further discrimination of the transition rate constants is possible.

For practical reasons it is important to limit the parameter-space in the computer-simulations to a manageable size. We therefore fixed the mobilities of the free state to the reference value obtained for the particular peptide (D_{free}), and the mobility of the bound state to the mobility of the TCR (D_{bound} = 0 µm^2/s). Trajectories were terminated at random with a trace-length distribution identical to the experimental data of the respective peptides. The only unknown parameters were therefore the bound fraction x_p, the characteristic duration of the bound state (τ_{off}), and the localization errors δ. We finally plotted the obtained p-values in two-dimensional parameter space (τ_{off} versus x_p). For each coordinate (x_p, τ_{off}) we have also simulated localization errors within a range $15nm < \delta < 70\ nm$; for display we showed only the maximum p-value obtained at the various settings of δ. By this, the test was slightly more permissive.

Monte Carlos simulations and Kolmogorov-Smirnov tests were implemented as described previously (3). In brief, off-lattice random walks were simulated in Matlab on a standard PC. We used $\#_{sub}$ substeps to simulate the molecular motion between two consecutive frames; $\#_{sub}$ was calculated according to $\#_{sub} = 10t_{del}/min(\tau_{off}, \tau_{on}, t_{del})$, thereby generating ten substeps for the shortest time-interval out of τ_{off}, τ_{on}, t_{del}. To assign the time-course of transitions between bound and free state of the tracer, a vector was generated of the form (D_{free}, D_{free}, D_{bound}, D_{bound}, D_{bound}, D_{free}, D_{free}, …), with every entry denoting the mobility for an individual substep. The substep length l_{sub} is defined by the diffusion constants via $l_{sub} = \sqrt{4Dt_{del}/\#_{sub}}$, and was distributed exponentially. The free tracer is characterized by the diffusion coefficient D_{free}, the bound tracer by D_{bound}. The start of the vector was chosen randomly with a probability specified by the bound fraction $x_p = \frac{\tau_{off}}{\tau_{on}+\tau_{off}}$. The duration of the individual states was calculated from an exponential distribution with the parameter τ_{off} (τ_{on}) for the bound (free) state. Localization errors were included by addition of Gaussian noise of mean zero and standard deviation δ to every position within the trajectory.

We used the Matlab function *kstest2* for the two-sample Kolmogorov-Smirnov hypothesis test.

2. Discussion

For our testing approach we assumed that the kinetics of both binding and unbinding is of first order, i.e. the lifetimes of the free and the bound state are exponentially distributed. In the following we provide arguments why this assumption is appropriate here, and draw further conclusions on the pMHC-TCR binding process within TCR microclusters.

Unbinding of pMHC from single TCR molecules

First order off-rates are generally assumed as the simplest model for protein interactions, and were also found to fit our data well. It should be noted that our model does not address the molecular binding process *per se*, but only discriminates between the free and the bound state. In particular, it could well be that a pMHC molecule rapidly rebinds the very same TCR molecule it has just left. Such rebinding, however, would be too fast to be captured at the applied time resolution >50 ms: a free pMHC molecule moves on average 370 nm between two consecutive images, which is twice the nearest neighbor distance of TCRs; the subsequent detectable encounter will thus be most likely with a different TCR molecule. Taken together, the reported bound state lifetimes can be interpreted as

effective lifetimes of pMHC before leaving the TCR, which may include rebinding on time-scales below 50 ms.

Binding of pMHC to (clustered) TCR

The binding of a mobile tracer to homogeneously distributed binding sites follows first order kinetics. During formation of the immunological synapse, however, one may expect the TCRs to become clustered at various length scales. In principle, our data include binding of pMHC to any TCR, irrespective whether it is inside a cluster or unassociated with a micro- or nanostructure. Interestingly, the data can be described perfectly by the simplest model of pMHC binding to homogeneously distributed TCRs in the contact zone; no indications for a significant subfraction with longer or shorter kinetics were observed. We argue in the flowing that a pMHC molecule binds most likely only once to a free TCR within a microcluster, and after unbinding leaves the microcluster. Consequentially, the diffusing pMHC molecules will bind randomly within the synapse, thereby justifying the assumption of first order kinetics.

First, rapid pMHC rebinding would be inconsistent with our previous FRET data, in which we found an on-rate of up to $0.015\ \mu m^2/(\mathrm{molec\ s})$ for (Cy5-MCC)MHC (1). The diffusion-limited on-rate is given by $k_{on} \sim 2\pi D_{free} = 4.3 \mu m^2/(\mathrm{molec\ s})$, two orders of magnitude faster. Thus, a microcluster needs to contain on average ~300 unoccupied TCR molecules to yield only one additional binding, which is highly unlikely under the applied conditions.

Second, rapid pMHC rebinding would be inconsistent with the quantitative agreement of the life-times reported here and in our previous single molecule FRET study. As pointed out above, it would not be possible to resolve the rapid succession of binding and unbinding events within a TCR microcluster with our method; therefore, even in the presence of multiple rebinding events in a TCR microcluster, we would have measured the rate constants for pMHC to leave the whole cluster. In contrast, the previous single molecule FRET experiments were performed at extremely low labeling conditions of the TCR, so that most TCR molecules did not carry a fluorophore; lifetimes determined by single molecule FRET thus referred to the single molecule unbinding event. The quantitative agreement thus indicates that pMHC does not show rapid rebinding.

A further consideration concerns the heterogeneity of on-rates. Indeed, in Huppa et al we reported differences in the in the on-rates within the IS, yielding hotspots of much higher binding affinities (1). In the analysis described here, we do not discriminate between different positions within the IS, therefore the results give average bound fractions and off-rates over the whole contact region.

Spatial heterogeneity within the synapse

In principle, the presented approach would allow for obtaining spatial information on the (un)binding kinetics. For example, it would be interesting to discriminate zones of high actin dynamics from zones with low morphological activity of the cell. Such analysis, however, would require recording much larger data sets, which would only be possible with automated single molecule imaging platforms.

Still, the obtained data sets allowed for testing whether there are systematic differences between the central and the peripheral regions of the synapse. In **Supporting Fig. 5A** and **B** we plotted the spatial profile of all trajectories included in the analysis of **Fig. 3C** and **D**. The distance r was measured between the cell center and the center of each trajectory. There is a slight decrease in the amount of data recorded in the cell center, which is a consequence of the experimental procedure: during the illumination sequence of 12 images, the synapse region is photobleached; the recovery of unbleached (Cy5-MCC)MHC from the cell surrounding generates the observed spatial profile. The decrease in data points for large r can be attributed to the decreasing number of cells with large diameter. Next, we plotted the spatial profile of the single molecule diffusion constant $\overline{D}$ (**Supporting**

Fig. 5C). Data within the first 5µm yielded identical diffusion constants, an increase in mobility at high radii could be indicative of lower affinity in the lamellipodial regions of the T cell due to increased cell membrane fluctuations.

3. References

1. Huppa, J. B., M. Axmann, M. A. Mortelmaier, B. F. Lillemeier, E. W. Newell, M. Brameshuber, L. O. Klein, G. J. Schütz, and M. M. Davis. 2010. TCR-peptide-MHC interactions in situ show accelerated kinetics and increased affinity. Nature 463:963-967.
2. Wieser, S., M. Moertelmaier, E. Fuertbauer, H. Stockinger, and G. J. Schutz. 2007. (Un)confined diffusion of CD59 in the plasma membrane determined by high-resolution single molecule microscopy. Biophys J 92:3719-3728.
3. Wieser, S., M. Axmann, and G. J. Schütz. 2008. Versatile analysis of single-molecule tracking data by comprehensive testing against Monte Carlo simulations. Biophys J 95:5988-6001.

4. Supporting Figures

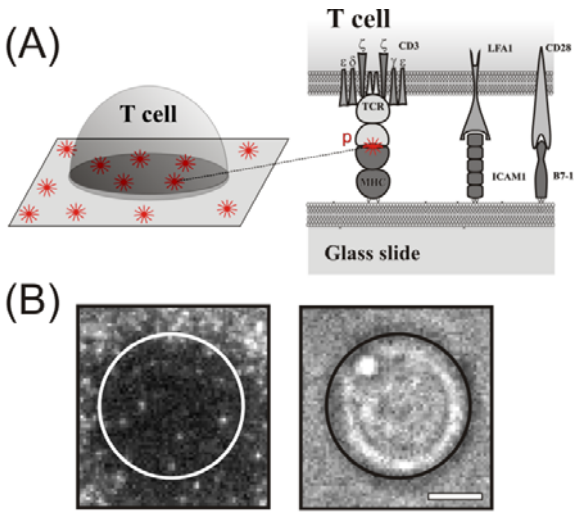

Supporting Figure 1. Principle of the method. (A) A supported lipid bilayer functionalized with ICAM1, B7-1 and (Cy5-p)MHC was used to mimic the plasma membrane of an antigen-presenting cell. Single molecule trajectories of (Cy5-p)MHC were recorded in the interface with a primary 5c.c7 T cell. (B) Fluorescence (left) and transmission light image (right) of a T cell on a functionalized lipid bilayer. The T cell perimeter was identified (black line) from the transmission light image and used for restricting the area of analysis in the fluorescence image (white line). Upon gentle photobleaching, single (Cy5-MCC)MHC molecules can be identified in the interface region. Scale bar = 4 µm.

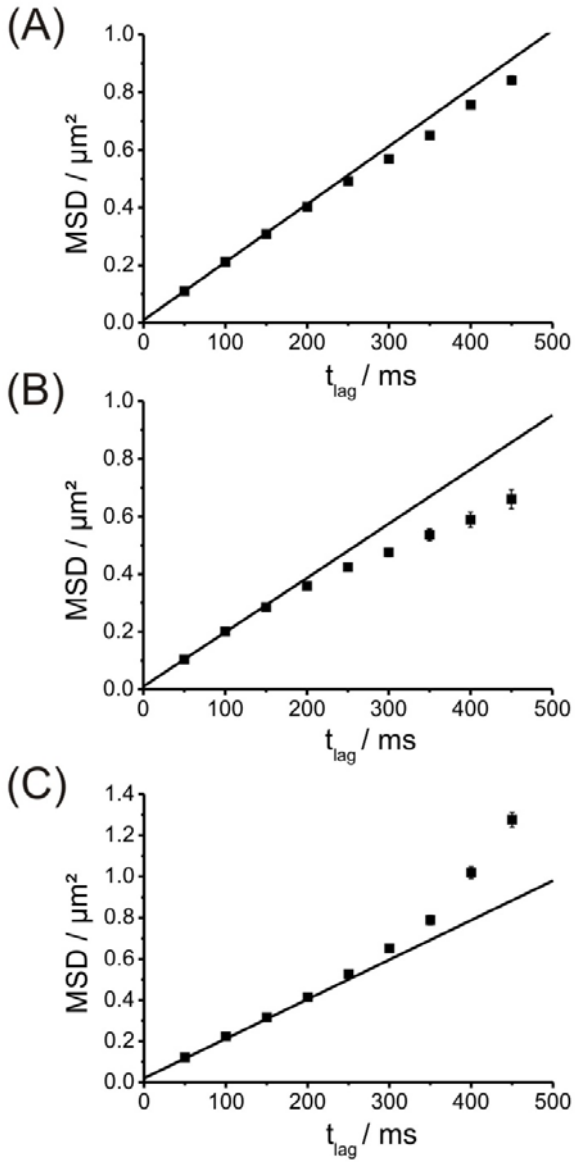

Supporting Figure 2. Mobility of non-stimulating peptides within the synapse under activating conditions. Diffusion was analyzed by plotting the mean square displacement (MSD) as a function of the time-lag t_{lag}. All data were recorded at a (Cy5-p)MHC surface density of 30 molec / µm² on a background of agonistic (Cy3-K5)MHC (30 molec / µm²); temperature was 33°C. In (**A**) we pooled (Cy5-p)MHC mobility data recorded outside the synapse including (Cy5-MCC)MHC, (Cy5-β2m)MHC, and (Cy5-T102S)MHC, yielding $D = 0.51\ \mu m^2/s \pm 0.01\ \mu m^2/s$. (**B**) and (**C**) show the same analysis for (Cy5-β2m)MHC and (Cy5-T102S)MHC recorded within the synapse, yielding $D_{\beta 2m} = 0.49\ \mu m^2/s \pm 0.01\ \mu m^2/s$ and $D_{T102S} = 0.48\ \mu m^2/s \pm 0.01\ \mu m^2/s$, respectively.

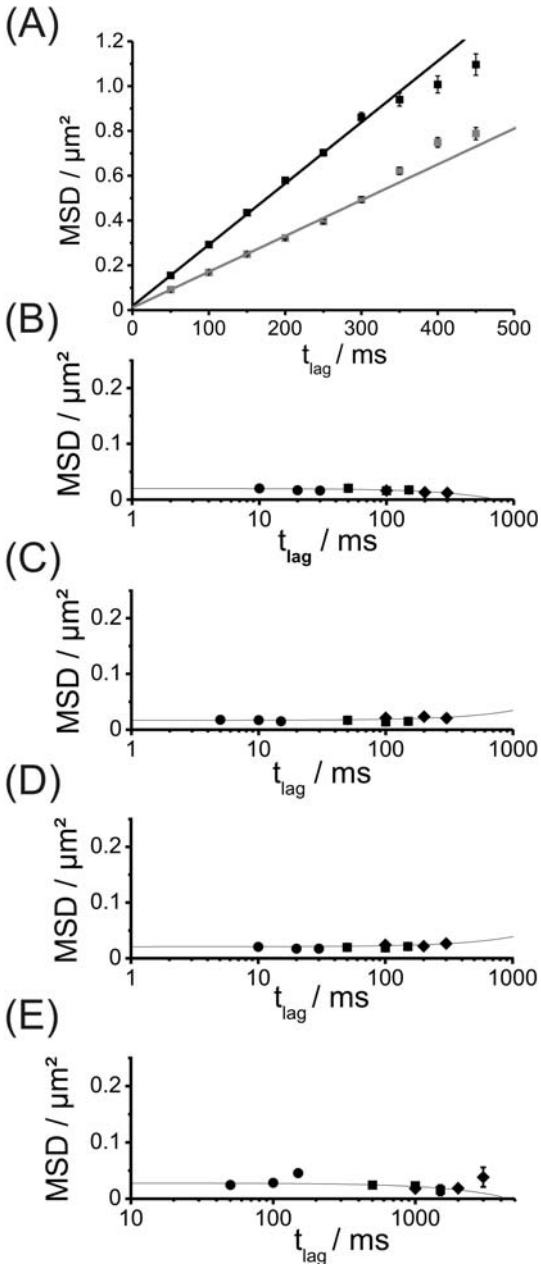

Supporting Figure 3. Mobility analysis of free and bound (Cy5-MCC)MHC. (**A**) shows exemplary data obtained for (Cy5-MCC)MHC measured within (gray) or outside (black) the interface of the bilayer with the T cell; data were recorded at 37°C. A linear fit yielded $D = 0.38\ \mu m^2/s \pm 0.01\ \mu m^2/s$ and $D_{free} = 0.68\ \mu m^2/s \pm 0.01\ \mu m^2/s$. (**B**-**E**) show the diffusion analysis of FRET events. Data were recorded at 37°C with $\sigma_{(Cy5-MCC)MHC} = 6\ molecules/\mu m^2$ (**B**), $30\ molecules/\mu m^2$ (**C**), and $150\ molecules/\mu m^2$ (**D**), or at 28°C with $\sigma_{(Cy5-MCC)MHC} = 30\ molecules/\mu m^2$ (**E**). For each experimental setting, the time-delay between two consecutive observations was varied between 5ms (●), 50ms (▪), and 100ms (♦). Diffusion constants were obtained from linear fits, yielding $D_{bound} = -0.007\ \mu m^2/s \pm 0.002\ \mu m^2/s$ (**B**), $D_{bound} = 0.004\ \mu m^2/s \pm 0.003\ \mu m^2/s$ (**C**), $D_{bound} = 0.004\ \mu m^2/s \pm 0.003\ \mu m^2/s$ (**D**), $D_{bound} = -0.002\ \mu m^2/s \pm 0.001\ \mu m^2/s$ (**E**).

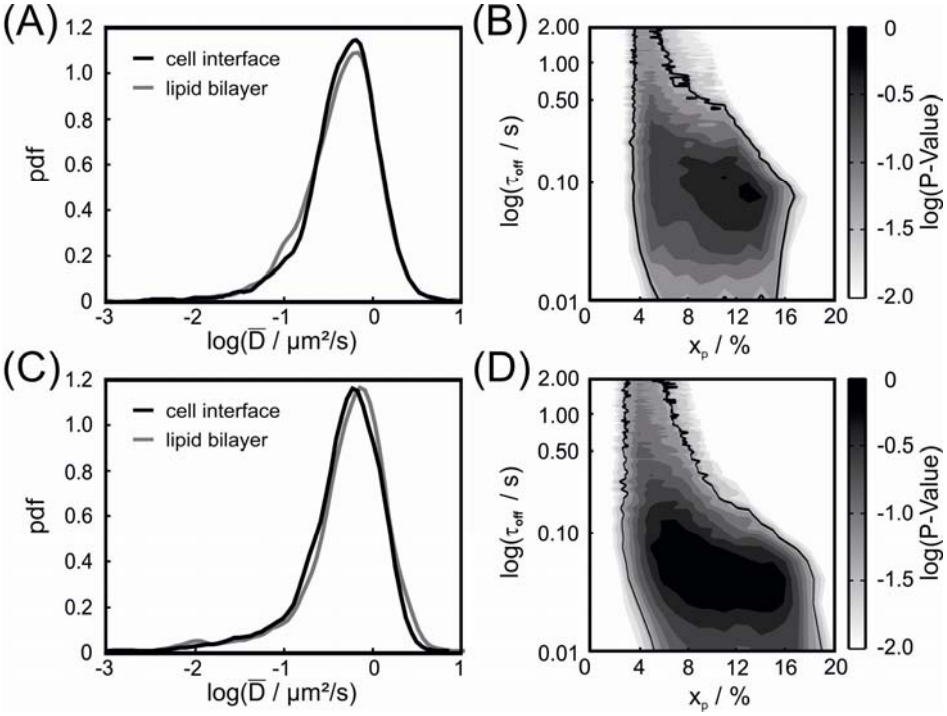

Supporting Figure 4. Analysis of the TCR interaction of (Cy5-β2m)MHC (**A, B**) and (Cy5-T102S)MHC (**C, D**). (**A**) and (**C**) show the probability distributions of $\overline{D}$ in the lipid bilayer / T cell interface (black), yielding only a weak difference compared to the mobility of the pMHC in the lipid bilayer outside the interface (gray). (**B**) and (**D**): The data sets were compared to comprehensive Monte Carlo simulations using the following fixed parameters for the simulations: D_{free} = 0.67 µm²/s (**B**) and D_{free} = 0.70 µm²/s (**D**) and, D_{bound} = 0 µm²/s. The 5% significance contour is indicated by a black line. For both peptides, bound fractions in a range $4\% \leq x_p \leq 18\%$ are consistent with the data, however, no conclusive statement is possible for the lifetime τ_{off}.

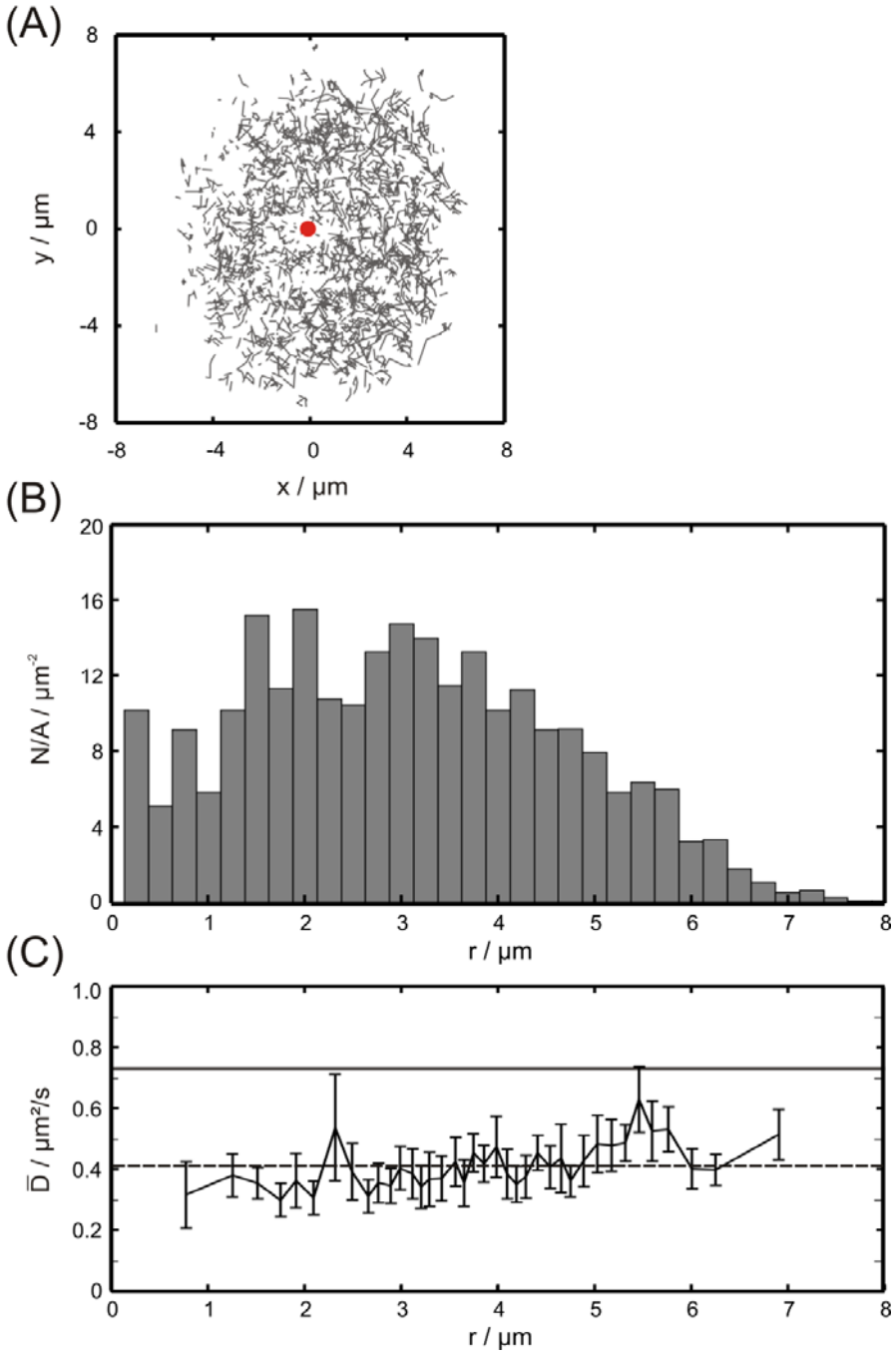

Supporting Figure 5. Analysis of the spatial profiles of the recorded data sets shown in Fig. 3C and D. (**A**) shows an overlay of 1250 trajectories recorded on 25 cells, plotted on a centralized coordinate frame; the red dot shows the center of the cells. (**B**) shows the same data as (**A**) plotted as surface densities versus distance from the cell center. The slight decrease in data density to the central region of the cells was due to enrichment of (Cy5-MCC)MHC in the central TCR-rich regions, which occasionally rendered unambiguous single molecule tracking impossible. (**C**) Single molecule diffusion constant $\overline{D}$ as a function of the distance from the cell center (sliding averages were taken over 30 data points). The mean $\overline{D}$ inside and outside the synapse are shown as dashed and full lines, respectively.

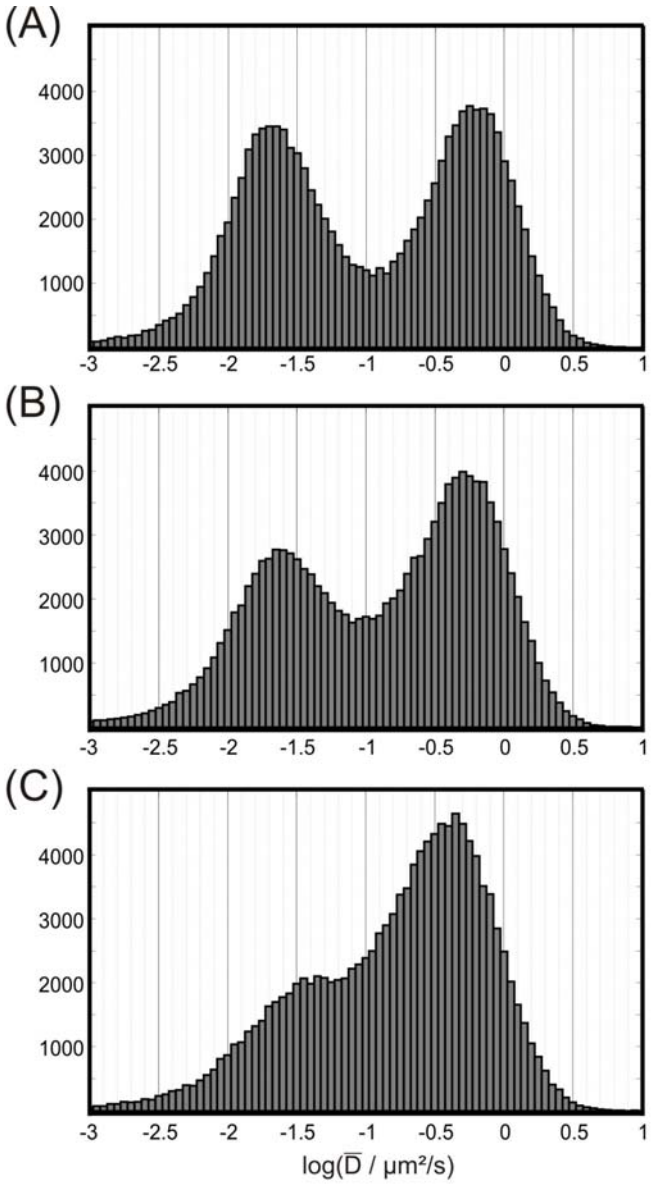

Supporting Figure 6. Histograms of simulated diffusion constants for the following parameter settings: bound fraction x_p=50%, localization errors δ=40nm, diffusion constants $D_{free} = 0.7\ \mu m^2/s$, $D_{bound} = 0\ \mu m^2/s$, the delay time between consecutive illumination was set to t_{lag}=50 ms. The lengths of the trajectories were distributed identically to the observed data (typical mean length was ~4.2 observations). Simulations were performed at $\tau_{on} = \tau_{off} = 1s$ (**A**), $\tau_{on} = \tau_{off} = 0.3s$ (**B**), and $\tau_{on} = \tau_{off} = 0.1\ s$ (**C**).

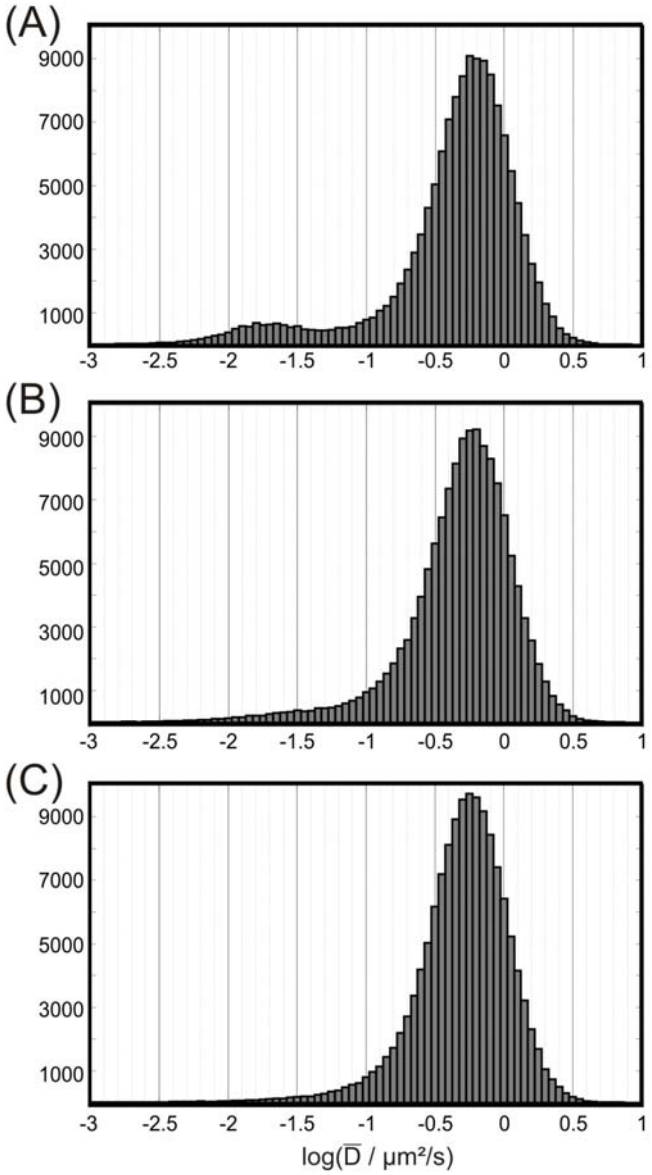

Supporting Figure 7. Histograms of simulated diffusion constants for the following parameter settings: bound fraction x_p=7%, localization errors δ=40nm, diffusion constants $D_{free} = 0.7\ \mu m^2/s$, $D_{bound} = 0\ \mu m^2/s$, the delay time between consecutive illumination was set to t_{lag}=50 ms. The lengths of the trajectories were distributed identically to the observed data (typical mean length was ~4.2 observations). Simulations were performed at $\tau_{on} = 13\ s$, $\tau_{off} = 1\ s$ (**A**); $\tau_{on} = 1.3\ s$, $\tau_{off} = 0.1\ s$ (**B**); $\tau_{on} = 0.13\ s$, $\tau_{off} = 0.01\ s$ (**C**).